UDK 669-153.6
Original scientific article/Izvirni znanstveni članek

ISSN 1580-2949
MTAEC9, 56(2)201(2022)

EFFECT OF COOLING RATE ON THE MICROSTRUCTURE AND MECHANICAL PROPERTIES OF SOLUTION-TREATED Mg-9Gd-4Y-2Zn-0.5Zr ALLOY

VPLIV HITROSTI OHLAJANJA NA MIKROSTRUKTURO IN MEHANSKE LASTNOSTI RAZTOPNO ŽARJENE ZLITINE Mg-9Gd-4Y-2Zn-0,5Zr

Zixuan Wang, Leichen Jia, Jie Zheng, Zhimin Zhang, Jianmin Yu, Xi Zhao, Yong Xue*

School of Materials Science and Engineering, North University of China, Taiyuan, China

Prejem rokopisa – received: 2021-11-15; sprejem za objavo – accepted for publication: 2022-02-23

doi:10.17222/mit.2021.317

Different cooling rates, such as room temperature water cooling (WQ), furnace cooling (FC), and water cooling + furnace cooling (FC +WQ), were introduced to study the effect on the solution-treated Mg-9Gd-4Y-2Zn-0.5Zr (*w*/%) alloy microstructure and mechanical properties. The grain size decreases as the cooling rate increases. With the lengthening of the cooling process time, the LPSO phase had enough time to nucleate and diffuse, the LPSO (long-period stacking order) phase filled the whole matrix crystal grains at the same time. In the process of furnace cooling and water cooling, the brightness of the LPSO phase was different, so it could be seen that the cooling rate would affect the contrast and morphology of the LPSO phase. The tensile yield strengths of the samples cooled with the furnace were better than those of the water-cooled samples, but their ultimate tensile strength and elongation to failure were poor. The fracture modes of the samples under different cooling rates were all subject to cleavage fracture, and the number and area of the cleavage planes and cleavage steps increased with the decrease of cooling speed, and the tearing area decreased, resulting in poor ultimate tensile strength and stretchability.

Keywords: cooling rate, solution treatment, microstructure, mechanical properties

Avtorji v tem članku opisujejo študijo vpliva hitrosti ohlajanja na mikrostrukturo in mehanske lastnosti raztopno žarjene zlitine Mg-9Gd-4Y-2Zn-0,5Zr (*w*/%). Izbrani postopki obdelave zlitine so bili: ohlajanje z vodo (WQ), ohlajanje v peči (FC) ter ohlajanje v vodi in peči (FC+WQ). Velikost kristalnih zrn zlitine se je zmanjševala z naraščanjem hitrosti ohlajanja. S podaljševanjem časa ohlajevanja je imela faza z dolgo periodo zlaganja (LPSO, angl.: long period stacking order) dovolj časa za nukleacijo in difuzijo in je LPSO tako istočasno lahko napolnila celotno matrico kristalnih zrn. V procesu ohlajanja v peči in ohlajanju z vodo je bila svetlost LPSO faze drugačna, kar pomeni, da je bila faza drugačna oziroma, da je hitrost ohlajanja vplivala na kontrast in morfologijo te faze. Natezna trdnost vzorcev ohlajenih v peči je bila boljša od tistih, ki so bili ohlajeni z vodo. Toda porušna natezna trdnost in raztezek preizkušancev sta bila oba zelo slaba. Način porušitve preizkušancev pri različnih načinih ohlajanja je bil pri vseh enak in sicer, prišlo je do cepilnega loma. Število cepilnih stopnic in ploskev ter njihov presek je naraščal z zmanjševanjem hitrosti ohlajanja preizkušancev. Zmanjševanje površine presekov cepljenja je posledično privedlo do poslabšanja natezne trdnosti in duktilnosti.

Ključne besede: hitrost ohlajanja, raztopno žarjenje, mikrostruktura, mehanske lastnosti

1 INTRODUCTION

Magnesium (Mg) and magnesium alloys have attracted more and more attention, and they are known as the best green materials in the 21st century because of their good physical and chemical properties.[1–3] However, traditional Mg alloys exhibited lower strength compared with other alloys, which hindered their wider application in engineering fields. In order to reflect the performance of magnesium alloys better, J. H. Zhang[4] defined high-strength magnesium alloys as those with an ultimate tensile strength (UTS) greater than 350 MPa, and magnesium-rare earth (Mg-RE) alloys were called the most promising high-strength magnesium alloys.[5–6] Adding rare-earth (RE) elements could effectively improve the mechanical behaviour of Mg alloys. It could be found from the related literature that the as-cast Mg alloys with an UTS greater than 350 MPa were Mg-RE alloys with gadolinium (Gd) as the main RE element. In recent years, it has been reported that increasing the content of yttrium (Y) in magnesium-yttrium-rare-earth (Mg-Y-RE) alloys can effectively improve the mechanical properties of the alloys, and the Y element has more excellent solid-solution strengthening efficiency compared to zinc (Zn), aluminium (Al) and many other elements. Hence, many kinds of research have also been carried out around Mg-Gd-Y-Zn-Zr alloys.[7–10] Especially, solid-solution strengthening as a major strengthening mechanism of Mg-RE alloys has received extensive attention from researchers.[11–15]

Dong Han et al. studied the effect of solution treatment on the microstructure and mechanical properties of the Mg-6Gd-3Y-1.5Zn-0.6Zr alloy and found that the growth of new layered long-period stacked ordered

*Corresponding author's e-mail:
yongxue395@163.com

phases from grain boundaries to internal grains could be observed after a solution treatment. The alloy exhibits excellent mechanical properties after being treated at 500 °C for 5 h.[16] C. Xu et al. pointed out that the Mg-8.2Gd-3.8Y-1.0Zn-0.4Zr alloy samples with furnace cooling showed a better tensile yield strength (YS), while the UTS and ductility were lower due to the formation of coarse grains and massive 14H-type long-period stacking ordered (14H-LPSO) phases.[17] L. Xiao et al. analyzed the microstructure evolution of the Mg-9.5Gd-0.9Zn-0.5Zr alloy during the cooling process in a furnace after solution treatment due to the non-uniform cooling rate in the furnace and found that cooling with the furnace to 420 °C was the optimal equilibrium condition for obtaining layered phase formation, fewer precipitated particles and inhibiting grain growth.[18]

However, few researchers[16] have studied the effect of different cooling rates on the microstructure and mechanical properties of the solid solution Mg-Gd-Y-Zn-Zr alloy in detail. In this paper, the cooling rate was controlled by controlling the degree of cooling with the furnace. The Mg-9Gd-4Y-2Zn-0.5Zr alloy was solution treated at (470, 500 and 530) °C for 8–24 h and then cooled with water cooling and furnace cooling, respectively. Furthermore, we studied in detail the microstructure and mechanical properties of the solid solution at 530 °C for 16 h after being cooled to different temperatures in the furnace.

2 EXPERIMENTAL PART

The Mg-9Gd-4Y-2Zn-0.5Zr ingots with a size of 440 mm in diameter and 660 mm in height were processed by semi-continuous casting. The specific chemical compositions of the alloy determined by inductively coupled plasma atomic emission spectrometry (ICP-AES) are displayed in **Table 1**. The solution treatment was carried out at (470, 500 and 530) °C for different times (8, 16, and 24) h, and then through room temperature water cooling and furnace, cooling to achieve the purpose of cooling. The average cooling rate with furnace cooling is 0.83 °C/min. At the same time, the samples that were solution treated at 530 °C for 16 h were cooled to (330, 390 and 450) °C with the furnace, respectively. A study of the melting temperature of the cast alloy eutectic phase via differential scanning calorimetry (DSC; TA DSC250) was made and its heating rate was 10 °C/min. So, to work over the microstructure evolution of the solution treatment at different cooling rates, firstly grinding and polishing with different grades of sandpapers and then polishing with 1.0 μm diamond polishing agent. The polished samples were corroded with acetic acid picric acid (1 g picric acid, 2 mL acetic acid, 2 mL distilled water and 14 mL alcohol) for 3–5 s. Using a optical microscope (OM; DM2500M, Leica Microsystems, Wetzlar, Germany) and a scanning electron microscope (SEM; SU5000, Hitachi, Tokyo, Japan) to observe the microstructure of the alloy. The chemical composition analysis was performed by energy-dispersive spectroscopy (EDS). The average grain size was measured using the linear-intercept method.

A bar with a diameter of 13 mm and a height of 80 mm was cut by electrical discharge wire-cutting and processed into tensile specimens with a working length of 25 mm and a diameter of 5 mm. At room temperature (T_R), the Instron 3382 tensile tester (INSTRON, Norwood, MA, USA) was used to obtain the tensile properties of the alloy at a strain rate of 0.008 mm/min and the fracture morphology was observed with a scanning electron microscope (SEM). In order to avoid the contingency of the results and reduce the error, each plan carried out tensile tests on three tensile specimens. The hardness of the as-cast Mg-9Gd-4Y-2Zn-0.5Zr alloy and solution-treatment alloy were measured on a Vickers hardness tester (UHL Vmht Mot Micro Hardness Tester), with a 200 N load and a 15 s loading time. Ten test data were taken for each sample, removing the maximum and minimum values and taking the average value to reduce the experimental error.

Table 1: The chemical composition of Mg-9Gd-4Y-2Zn-0.5Zr alloy

Element	Gd	Y	Zn	Zr	Si	Cu	Mg
w/%	9.48	4.00	1.98	0.50	< 0.01	< 0.01	Bal.

3 RESULTS AND DISCUSSION

3.1 Microstructure

3.1.1 As-cast alloy

The DSC curve of as-cast Mg-9Gd-4Y-2Zn-0.5Zr alloy is in **Figure 1**. It shows that the first peak temperature of the endothermic reaction was 530.7 °C, the second peak temperature was 534.6 °C, and the initial melting temperature of the second phase was 523.9 °C. According to related literature,[19–20] when there were multiple peaks in the peak temperature of the DSC curve, the

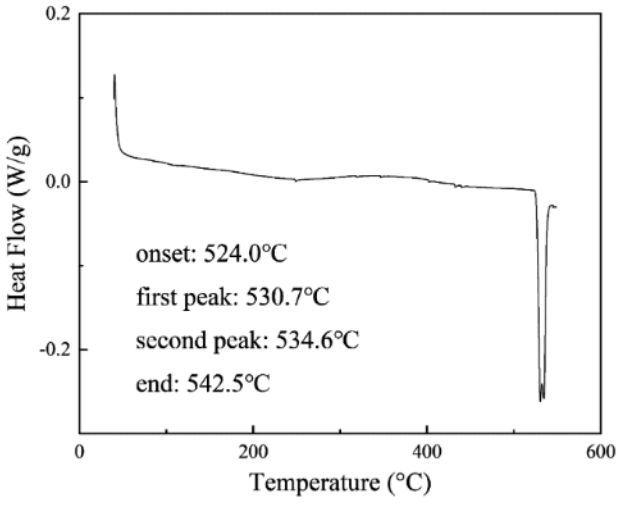

Figure 1: DSC curvilineal of the as-cast Mg-9Gd-4Y-2Zn-0.5Zr alloy

last peak should prevail and the peak temperature should be taken as the peak temperature. And based on experience, generally, the highest value of the solid solution temperature was about 5 °C lower than the peak temperature of the eutectic phase. Therefore, the solution-treatments temperature in this paper was determined at (470, 500 and 530) °C.

Figure 2 shows the as-cast microstructure of the Mg-9Gd-4Y-2Zn-0.5Zr alloy. It can be seen that the as-cast alloy with an average grain size of (71 ± 2) μm is mainly composed of α-Mg matrix and network-distributed eutectic organizational composition. The eutectic phase was distributed at the grain boundary with obvious skeletal characteristics. This was due to the high cooling rate in the casting process of the RE-Mg alloy with a high RE content, and the high melting point RE compounds formed by the RE elements and α-Mg matrix did not have enough diffusion time, so that a large amount of segregation generated at the grain boundary and formed a eutectic structure.[21–23] It could be seen that the eutectic structure was composed of a bright part and a grey part from **Figure 2b**. Their chemical compositions were the same according to the EDS analysis results of **Figures 2d** and **2e**. The Mg : Gd (Y, Zn) ratio of the bright part was 77.36 : 11.11 (11.54), which was close to that of Mg_5Gd (Y, Zn) phase. And the Mg : (Gd, Y) Zn ratio of a grey part was 88.31 : 6.80 (4.89), which was close to that of Mg_{12} (Gd, Y) Zn phase. It can be seen that some fine, massive particles were scattered at grain boundaries and inside the grain from **Figure 2a**. These particles are RE-rich phases, according to **Figure 2c**. At the same time, it could be found that there were lamellar phases arranged uniformly and parallel to each other near the grain boundary in **Figure 2b**. According to the comprehensive analysis in **Figure 2e**, it could be obtained that it was a solidified short layered phase, which was the LPSO (long-period stacking order) phase. The formation of the LPSO phase required abundant RE phase and Zn, and the plenty of RE phase and Zn element were distributed in a large amount at the crystal boundary, so we could find that the lamellar phases were distributed at the boundaries and extended into the grains. The lamellar phase in these as-cast alloys was considered to be a metastable LPSO phase, because it did not have the structure of 14H-LPSO, in the strictest sense, but had its characteristics, which produced a stable 14H-LPSO structure in the subsequent solution treatment.[24] The metastable 14H-LPSO phase has the same stacking sequence ABCA as the steady 14H-LPSO phase, but the building blocks of the metastable 14H-LPSO phase include different numbers of Mg layers (two Mg layers and three Mg layers), and the stable 4H-LPSO phase has only three Mg layers.[25]

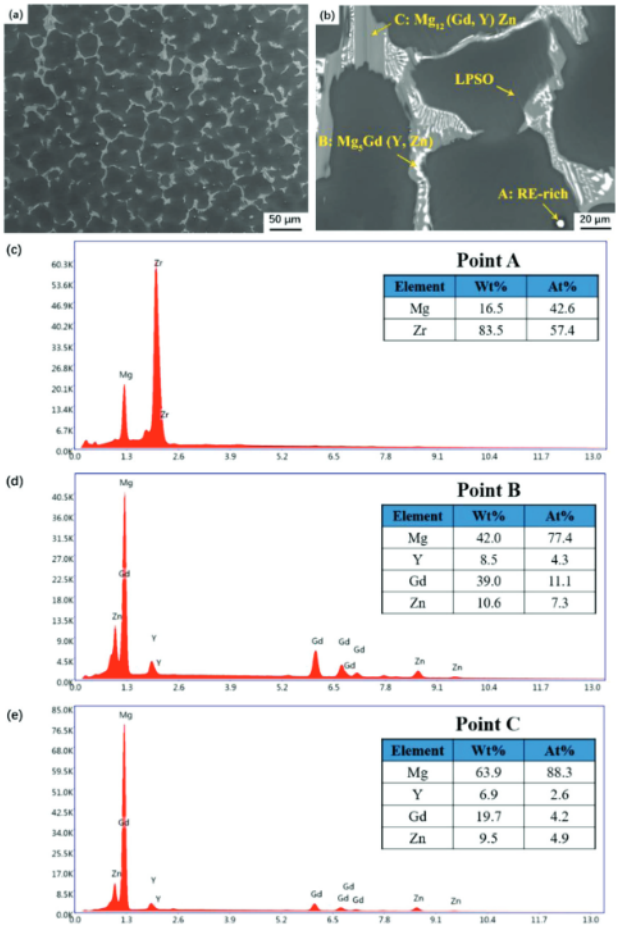

Figure 2: Microstructure of the as-cast Mg-9Gd-4Y-2Zn-0.5Zr alloy (a and b), EDS results (c, d and e) of the phases marked A, B and C in (b)

3.1.2 Alloy solution treated at different temperatures

The layered structure in the as-cast alloy first dissolved into the Mg matrix and disappeared during the solution treatment, and then the new layered structure was caused by dislocations of high density at the grain boundaries and the profuse RE and Zn atoms.[26] And the new structure increased with the increase of the solution treatment time. **Figure 3** shows the microstructures of the alloy after a solution treatment at different temperatures for 24 h after water cooling and furnace cooling, respectively. **Figures 3a, 3c** and **3e** are the light-microscope images after solution treatments at (470, 500 and 530) °C for 24 h and water quenched (WQ). The grain sizes are (80 ± 2) μm, (83 ± 2) μm and (95 ± 3) μm respectively. It can be seen that the grain size increased as the temperature increases. At the same time, the newly generated lamellar phase, which is the 14H-LPSO phase, would also increase with an increase in the temperature.[21] The 14H-LPSO phase was generated at the grain boundary first, distributed in parallel along the grain boundary and gradually extending into the grain. They had the same arrangement direction in the same grain, and the orientations of the LPSO within the different grains were inconsistent. In addition, it can be seen from the figure that the second phase continued to thicken along the grain boundaries and the shape changed into

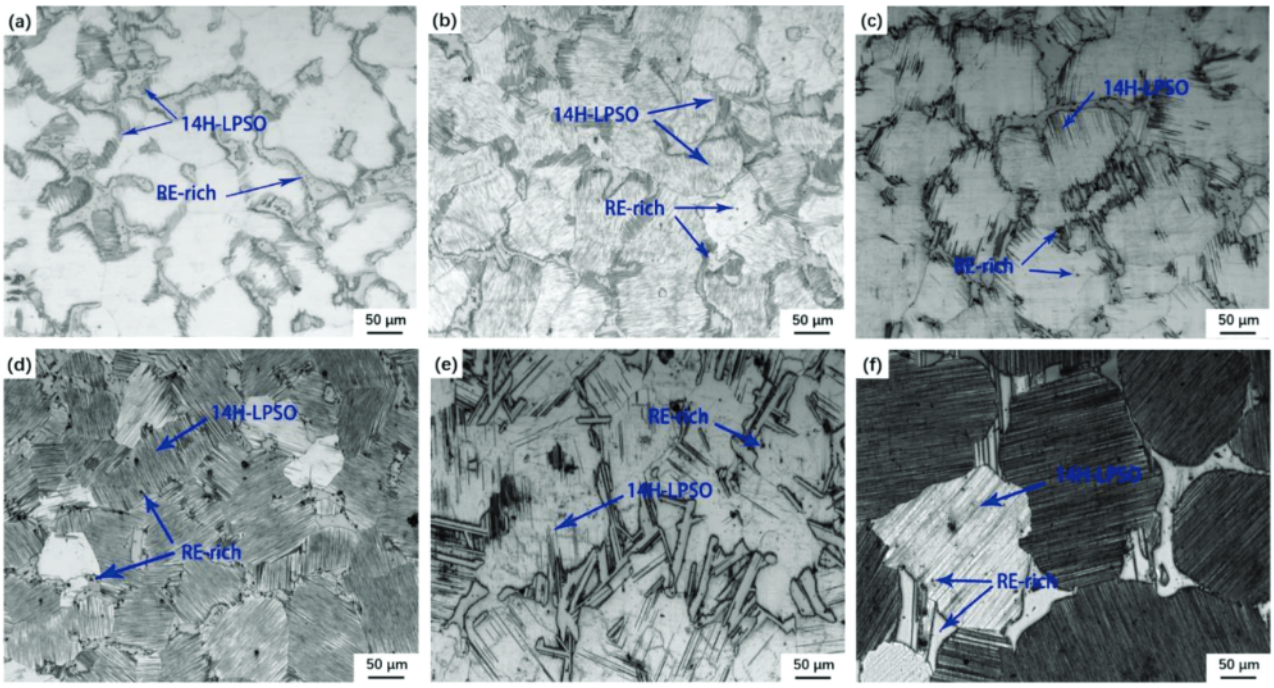

Figure 3: Optical micrographs of the Mg-9Gd-4Y-2Zn-0.5Zr alloys solution treated for 24 h: a) 470 °C + WQ, b) 470 °C + FC, c) 500 °C + WQ, d) 500 °C + FC, e) 530 °C + WQ, f) 530 °C + FC

strips as the temperature increased, this was especially obvious at 530 °C. With the increase of the solution-treatment temperature, the number of fine particles randomly dispersed inside the grains and at the grain boundaries gradually increases. These particles were called RE-rich phases, which were produced by high-temperature heat treatment, and their formation might be divided into two reasons:

(1) precipitation from the supersaturated α-Mg matrix,

(2) eutectic phase during heat-treatment decomposition.[17]

Figures 3b, 3d and **3f** were respectively the light-microscope images after solution treatment at (470, 500 and 530) °C for 24 h after furnace cooling (FC). The grain size was (92 ± 4) μm, (93 ± 4) μm and (151 ± 5) μm, respectively. The furnace cooling and water cooling had the same point that the crystal grain size increased with the increasing of temperature. But the crystal grain size after the furnace cooling at the same temperature was larger than that after the water cooling. The grain growth was more obvious with the furnace cooling. **Figure 4** shows the bar chart of grain size of samples under different states. It can be clearly seen that the abnormal grain growth would be caused by furnace cooling after solution treatment at 530 °C for 24 h. Compared with water cooling with furnace cooling, more layered phases formed and covered the entire grains, and the amount of RE-rich phases precipitated reduced. As the cooling rate decreases, the RE element and Zn atoms diffused into the matrix, the lamellar phase had enough time to nucleate and diffuse, and the lamellar phase covered the whole grains. In the comparison of different temperatures with the cooling state of the furnace, the number of precipitated phases at 500 °C was the largest. Compared with the water quenching, the RE-rich phases after the furnace cooling were randomly distributed at the grain boundaries and within the grains, while most of the RE-rich phases after water cooling were distributed at the grain boundaries. Moreover, the amount of RE-rich phases after the furnace cooling was less than that after the water cooling. According to research,[27] these fine RE-rich particle phases had the effect of grain refinement on inhibiting the growth of grains. Therefore, this was also the reason why the grain size after water cooling was smaller than that after cooling with the furnace.

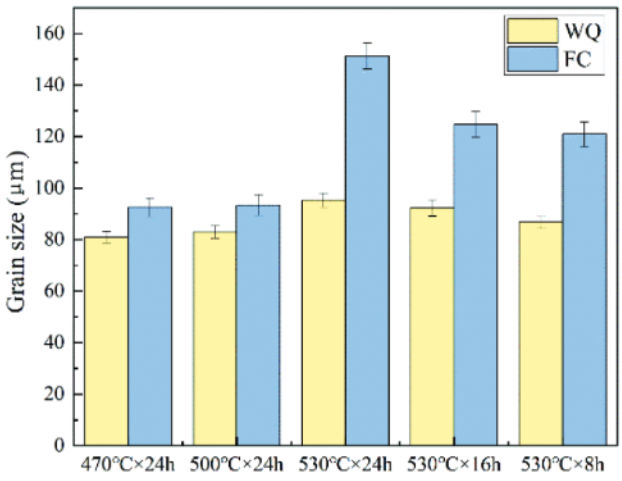

Figure 4: Grain size of different samples

3.1.3 Alloy solution treated at the same temperatures

Figure 5 shows the SEM images of the microstructure of the alloy after solution treatment at 530 °C for (8, 16 and 24) h after water quenching (WQ) and furnace cooling (FC), respectively. The grain sizes of **Figures 5a**, **5c**, and **5e** are (87 ± 2) μm, (92 ± 3) μm and (95 ± 4) μm. It can be seen that the second phase became strip and became coarser and longer with the increase of time, and the lamellar phase became more and more after solution treated at 530 °C by water quenching. The grain size of **Figures 5d**, **5e** and **5f** is (121 ± 5) μm, (125 ± 5) μm and (151 ± 6) μm, respectively. The grain growth was obvious, and the strip-shaped second phase was also very coarse as the grains grew. Compared with the water cooling, the number of RE-rich particles had become very small, resulting in the growth of crystal grains. Through the image comparison between water cooling and furnace cooling, it could be concluded that the LPSO phase after water cooling was brighter in the SEM image. That was to say that the layers formed during the furnace-cooling process were thinner than the LPSO phase formed after water cooling.[28,29] Therefore, we could draw a conclusion that the cooling rate affected the contrast and morphology of the lamellar phase. According to other people's studies, the 14H-LPSO phase produced during the furnace cooling process belongs to the metastable LPSO phase, which had a lower thermal stability, although the stacking order was the same as 14H-LPSO, it was not strictly in the sense the 14H-LPSO structure.[30,31] The higher the solution temperature and the longer the time, the better the solution effect, but due to the abnormal grain growth at 530 °C solution treated for 24 h, the solution treatment at 530 °C for 16 h is the best solution. The effect of different cooling rates on the alloy was studied. Accordingly the cooling rate was controlled at different temperatures as the furnace cools to different temperatures. **Figures 6a** to **6c** show SEM images of furnace cooling to different temperatures after a solid-solution treatment at 530 °C for 16 h. **Figure 7** shows the broken line chart of grain size

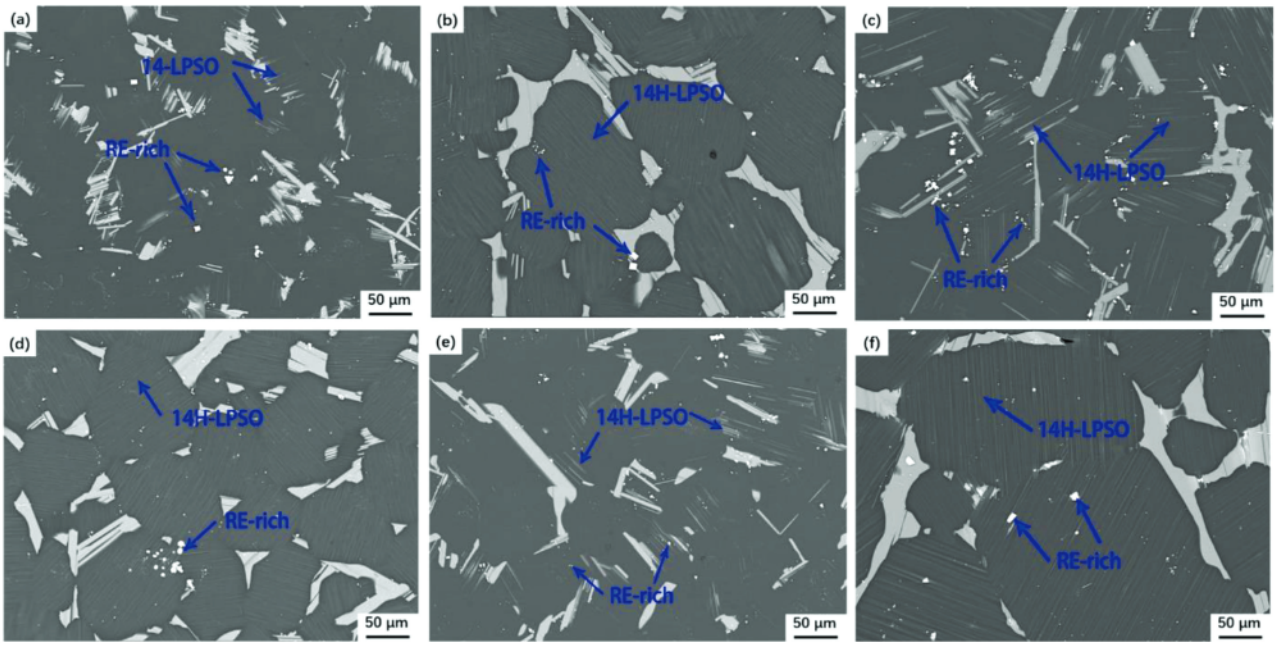

Figure 5: SEM images of the Mg-9Gd-4Y-2Zn-0.5Zr alloys solution treated at 530 °C: a) 8 h + WQ, b) 8 h + FC, c) 16 h + WQ, d) 16 h + FC, e) 24 h + WQ, f) 24 h + FC

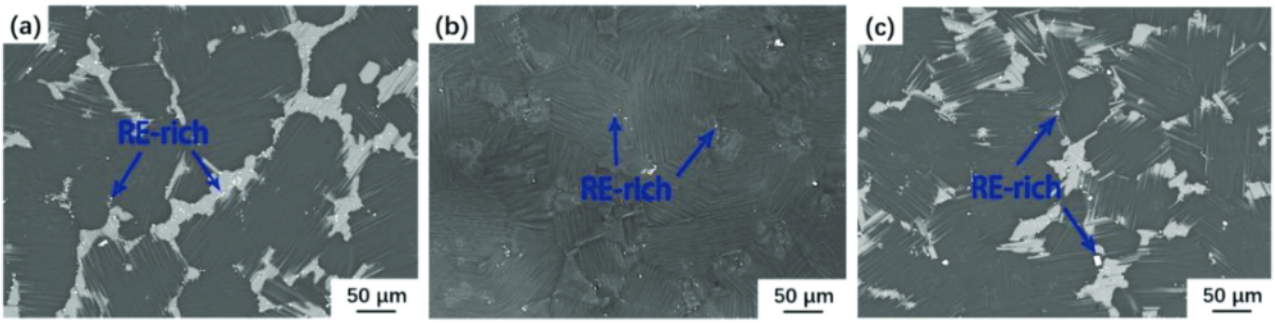

Figure 6: SEM images of Mg-9Gd-4Y-2Zn-0.5Zr alloy solution treated at 530 °C for 16 h and then furnace cooled to: a) 330 °C, b) 390 °C, c) 450 °C

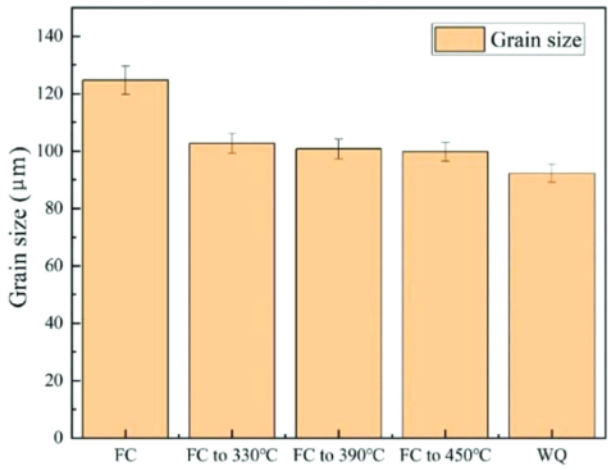

Figure 7: Grain size obtained after solution treatment at 530 °C for 16 h for different cooling procedures

after solid-solution treatment at 530 °C for 16 h. The abscissa is the cooling rate from slow to fast. We found that the number of RE-rich particles increases, which led to a decrease of the grain size with an increase of the cooling rate.

3.2 Mechanical properties

Table 2 shows the tensile yield strength (YS), ultimate tensile strength (UTS) and elongation to failure for each sample measured by a tensile test at room temperature and the hardness measured by a durometer at room temperature. The YS of the samples decreased as the cooling rate increased. In order to study the change of the YS with the cooling rate more accurately, this paper added the cooling rate between the furnace cooling and room temperature water cooling to control the cooling rate. Therefore, we found that the YS first decreased and then slowly increased with the increasing of the cooling rate, but the increasing was relatively small. The elastic modulus and hardness of the LPSO phase were high, and the main deformation mode (0001) substrate slip of the Mg alloy dominated the shaping action of the LPSO phase, so the lamellar LPSO phase played a role as a funicle reinforcing agent to obtain the reinforced alloy.[32]

Therefore, as the decrease of the cooling rate during cooling, the layered precipitates increased and became full of grains under the action of heat driving, resulting in the YS of the samples cooled with the furnace being higher than that of the water-cooled samples. The UTS of the sample after solution treatment was improved, and the UTS also increased with the increase of the cooling rate. The elongation increased as the cooling rate increased. **Figure 8** shows the SEM image of the fracture surface of the sample. We could know that no matter what the cooling rate was, there were cleavage steps, cleavage facets, dents and tear ridges on the fracture surface. From this it can be concluded that the fracture modes were all quasi-cleavage fracture. **Figures 8a** to **8d** were compared. **Figures 8b** and **8d** have more cleavage facets and cleavage steps than **Figures 8a** and **8c**. And cleavage facets and cleavage steps became larger as the grain size increased, and there were a few dimples and tear ridges, which resulted in poor extensibility of the samples after cooling with the furnace. The hardness was not significantly affected by the cooling rate, but in detail, it appeared that the hardness and the cooling rate were negatively correlated. Combining all the data, the mechanical properties obtained by water cooling after solution treatment at 500 °C for 24 h was the best. The poor tensile properties obtained after solution treatment at 530 °C for 24 h followed by furnace cooling were due to the abnormal growth of the crystal grains. The mechanical properties of the sample after the solution treatment were mainly related to the grain size and the content of the second phase.[33] The grain size of the water-cooled sample after the solution treatment at 500 °C for 24 h had grown a little normal according to the law, and the second phase precipitates had changed. Multi-consolidation played the role of solid-solution atoms, and the obvious second-phase strengthening occurred. The layered LPSO phase dispersed at the grain boundary and into the grain, hindering the movement of dislocations so as to increase the strength, and the coordinated deformation ability of the LPSO made it possible to improve the strength, while ensuring good shaping.[16]

Table 2: Mechanical properties of different samples

Samples	Yield strength (MPa)	Ultimate tensile strength (MPa)	Elongation to failure (%)	Hardness (HV)
As-cast	120.8	201.4	3.30	81.0
500 °C × 24 h + FC	150.6	218.8	4.31	87.6
500 °C × 24 h + WQ	126.1	237.6	5.70	82.0
530 °C × 24 h + FC	123.7	204.5	0.63	87.8
530 °C × 24 h + WQ	79.7	209.4	1.64	81.4
530 °C × 16 h + FC	115.5	206.0	1.44	93.8
530 °C × 16 h + FC to 330 °C	77.0	215.6	3.50	92.0
530 °C × 16 h + FC to 390 °C	81.9	220.1	4.60	90.0
530 °C × 16 h + FC to 450 °C	84.0	225.0	4.80	86.1
530 °C × 16 h + WQ	84.9	221.6	5.44	85.5

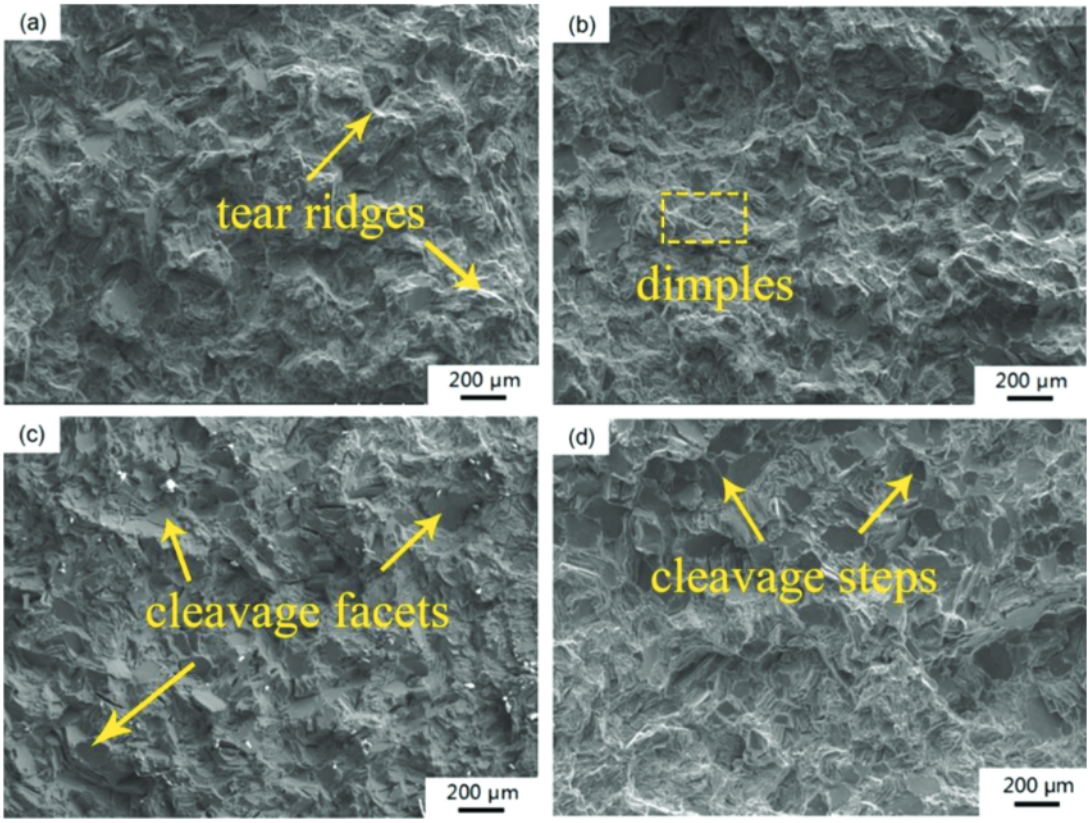

Figure 8: SEM images of fractured tensile samples after solution treated for 24 h at: a), 500 °C + WQ, b) 500 °C + FC, c) 530 °C + WQ, d) 530 °C + FC

4 CONCLUSIONS

The Mg-9Gd-4Y-2Zn-0.5Zr (*w*/%) alloy was solution treated at 470–530 °C for 8–24 h, and then cooled with water at room temperature and cooled with a furnace. At the same time, the samples were solid-solution treated at 530 °C for 16 h. Carrying out different degrees of furnace cooling, and finally carrying out the study of microstructure and mechanical properties. The results of the study were shown below:

1) As the temperature increased under different cooling rates, the grain size increased. The grain size decreased with the increasing of the cooling rate. This was due to the increase in the number of RE-rich phase particles. The fine RE-rich particles had the role of inhibiting grain growth.
2) As the cooling rate decreased, the RE and Zn atoms dispersed into the matrix, and the lamellar phase had enough time to nucleate and diffuse, and covered the matrix crystal grains.
3) The fracture modes at different cooling rates were all quasi-cleavage fractures. The only difference was that the cleavage steps and the inside of the solution would increase with the decrease of the cooling rate, and the tear zone and dents would decrease. The yield strength decreased with the increase of the cooling rate. The ultimate tensile strength of the sample after solution treatment was improved, and the ultimate tensile strength also increased with the increase of the cooling rate. The elongation increased as the cooling rate increased.
4) The hardness was not significantly affected by the cooling rate, but the hardness slowly decreased as the cooling rate increased.

Acknowledgment

The study was supported by the National Natural Science Foundation of China (Grant No. 52075501) and Magnesium alloy high-performance XXX multi-directional extrusion technology (JCKY2018408B003).

5 REFERENCES

[1] Y. Yang, X. M. Xiong, J. Chen, X. D. Peng, D. L. Chen, F. S. Pan, Research advances in magnesium and magnesium alloys in 2020, J. Magnes. Alloy, 9 (**2021**), 705–747, doi:10.1016/j.jma.2021.04.001

[2] T. C. Xu, Y. Yang, X. D. Peng, J. F. Song, F. S. Pan, Overview of advancement and development trend on magnesium alloy, J. Magnes. Alloy, 7 (**2019**) 3, 536–544, doi:10.1016/j.jma.2019.08.001

[3] J. F. Song, J. She, D. L. Chen, F. S. Pan, Latest research advances on magnesium and magnesium alloys worldwide, J. Magnes. Alloy, 8 (**2020**) 1, 1–41, doi:10.1016/j.jma.2020.02.003

[4] J. S. Xie, J. H. Zhang, Z. H. You, S. J. Liu, K. Guan, R. Z. Wu, J. Wang, J. Feng, Towards developing Mg alloys with simultaneously improved strength and corrosion resistance via RE alloying, J. Magnes. Alloy, 9 (**2021**) 1, 41–56, doi:10.1016/j.jma.2020.08.016

[5] H. C. Pan, Y. P. Ren, H. Fu, H. Zhao, L. Q. Wang, X. Y. Meng, G. W. Qin, Recent developments in rare-earth free wrought magnesium alloys having high strength: A review, J. Alloys Compd., 663 (**2016**), 321–331, doi:10.1016/j.jallcom.2015.12.057

[6] S. H. You, Y. D. Huang, K. U. Kainer, N. Hort, Recent research and developments on wrought magnesium alloys, J. Magnes. Alloy, 5 (**2017**) 3, 239–253, doi:10.1016/j.jma.2017.09.001

[7] K. Luo, L. Zhang, G. H. Wu, W. C. Liu, W. J. Ding, Effect of Y and Gd content on the microstructure and mechanical properties of Mg-Y-RE alloys, J. Magnes. Alloy, 7 (**2019**) 2, 345–354, doi:10.1016/j.jma.2019.03.002

[8] B. Li, B. G. Teng, G. X. Chen, Microstructure evolution and mechanical properties of Mg-Gd-Y-Zn-Zr alloy during equal channel angular pressing, Mater. Sci. Eng., A, 744 (**2019**), 396–405, doi:10.1016/j.msea.2018.12.024

[9] C. Xu, S. W. Xu, M. Y. Zheng, K. Wu, E. D. Wang, S. Kamado, G. J. Wang, X. Y. Lv, Microstructures and mechanical properties of high-strength Mg–Gd–Y–Zn–Zr alloy sheets processed by severe hot rolling, J. Alloys Compd., 524 (**2012**), 46–52, doi:10.1016/j.jallcom.2012.02.050

[10] Q. Yang, B. L. Xiao, Q. Zhang, M. Y. Zheng, Z. Y. Ma, Exceptional high strain rate superplasticity in Mg-Gd-Y-Zn-Zr alloy with long period stacking ordered phase, Scr. Mater., 69 (**2013**) 11–12, 801–804, doi:10.1016/j.scriptamat.2013.09.001

[11] J. H. Zhang, S. J. Liu, R. Z. Wu, L. G. Hou, M. L. Zhang, Recent developments in high-strength Mg-RE-based alloys: Focusing on Mg-Gd and Mg-Y systems, J. Magnes. Alloy, 6 (**2018**) 3, 277–291, doi:10.1016/j.jma.2018.08.001

[12] X. Z. Jin, W. C. Xu, Z. Z. Yang, C. Yuan, D. B. Shan, B. G. Teng, B. C. Jin, Analysis of abnormal texture formation and strengthening mechanism in an extruded Mg-Gd-Y-Zn-Zr alloy, J. Mater. Sci. Technol., 45 (**2020**), 133–145, doi:10.1016/j.jmst.2019.11.021

[13] B. Li, B. G. Teng, W. C. Xu, Hot Deformation Characterization of Homogenized Mg-Gd-Y-Zn-Zr Alloy During Isothermal Compression, JOM, 71 (**2019**), 4059–4070, doi:10.1007/s11837-019-03556-y

[14] X. J. Zhou, Y. Yao, J. Zhang, X. M. Chen, W. Y. Huang, J. Pan, H. R. Wang, M. P. Weng, A high-performance Mg-4.9Gd-3.2Y-1.1Zn-0.5Zr alloy via multidirectional forging after analyzing its compression behaviour, J. Mater. Sci. Technol., 70 (**2021**), 156–167, doi:10.1016/j.jmst.2020.08.054

[15] X. J. Zhou, C. M. Liu, Y. H. Gao, S. N. Jiang, Z. Y. Chen. Mechanical Properties of the Mg-Gd-Y-Zn-Zr Alloys with Different Morphologies of Long-Period Stacking Ordered Phases, J. Master. Eng. Perform., 27 (**2018**), 6237–6245, doi:10.1007/s11665-018-3713-z

[16] D. Han, H. M. Chen, Q. H. Zang, Y. X. Qian, H. W. Cui, L. Wang, J. Zhang, Y. X. Jin, Effect of solution treatment on microstructure and properties of Mg-6Gd-3Y-1.5Zn-0.6Zr alloy, Mater. Charact., 163 (**2020**), 110295, doi:10.1016/j.matchar.2020.110295

[17] C. Xu, M. Y. Zheng, K. Wu, E. D. Wang, G. H. Fan, S. W. Xu, S. Kamado, X. D. Liu, G. J. Wang, X. Y. Lv, Effect of cooling rate on the microstructure evolution and mechanical properties of homogenized Mg-Gd-Y-Zn-Zr alloy, Mater. Sci. Eng., A, 559 (**2013**), 364–370, doi:10.1016/j.msea.2012.08.112

[18] L. Xiao, G. Y. Yang, H. Qin, J. Q. Ma, W. Q. Jie, Microstructure evolution and quench sensitivity characterizations of Mg-9.5Gd-0.9Zn-0.5Zr alloy, Vacuum, 181 (**2020**), 109651, doi:10.1016/j.vacuum.2020.109651

[19] Y. Cui, Y. S. Shi, J. Zheng, Z. M. Yan, J. S. Zhang, Z. M. Zhang, Q. Wang, Y. Xue, Influence of heat treatment on the tensile properties and fatigue properties of Mg-8.8Gd-3.5Y-1.5Zn-0.5Zr alloy, Mater. Res. Express, 8 (**2021**), 056518, doi:10.1088/2053-1591/ac00f1

[20] J. Zheng, Z. M. Yan, J. S. Ji, Y. S. Shi, H. Zhang, Z. M. Zhang, Y. Xue, Effect of heat treatment on mechanical properties and microstructure evolution of Mg-9.5Gd-4Y-2.2Zn-0.5Zr alloy, J. Magnes. Alloy, 7 (**2021**), 1–9, doi:10.1016/j.jma.2021.05.018

[21] K. Yamada, Y. Okubo, M. Shiono, H. Watanabe, S. Kamado, Y. Kojima, Alloy Development of High Toughness Mg-Gd-Y-Zn-Zr Alloys, Mater. Trans., JIM, 47 (**2006**), 1066–1070

[22] X. X. Wei, L. Jin, S. Dong, F. H. Wang, J. Dong, Effect of Zn / (Gd + Y) ratio on the microstructure evolution and mechanical properties of Mg-Gd-Y-Zn-Zr alloy Mater. Charact., 169 (**2020**), 110670, doi:10.1016/j.matchar.2020.110670

[23] S. Zhang, G. Y. Yuan, C. Lu, W. J. Din, The relationship between $(Mg, Zn)_3RE$ phase and 14H-LPSO phase in Mg-Gd-Y-Zn-Zr alloys solidified at different cooling rates, J. Alloys Compd., 509 (**2011**), 3515–3521, doi:10.1016/j.jallcom.2010.12.136

[24] C. Xu, M. Y. Zheng, Y. Q. Chi, X. J. Chen, K. Wu, E. D. Wang, G. H. Fan, P. Yang, G. J. Wang, X. Y. Lv, S. W. Xu, S. Kamado, Microstructure and mechanical properties of the Mg-Gd-Y-Zn-Zr alloy fabricated by semi-continuous casting, Mater. Sci. Eng., A, 549 (**2012**), 128–135, doi:10.1016/j.msea.2012.04.018

[25] X. J. Zhou, C. M. Liu, Y. H. Gao, S. N. Jiang, X. Z. Han, Z. Y. Chen, Evolution of LPSO Phases and Their Effect on Dynamic Recrystallization in a Mg-Gd-Y-Zn-Zr Alloy, Metall. Mater. Trans. A, 48 (**2017**), 3062–3072, doi:10.1007/s11661-017-4081-2

[26] C. Xu, M. Y. Zheng, S. W. Xu, K. Wu, E. D. Wang, S. Kamado, G. J. Wang, X. Y. Lv, Microstructure and mechanical properties of rolled sheets of Mg-Gd-Y-Zn-Zr alloy: As-cast versus as-homogenized, J. Alloys Compd., 528 (**2012**), 40–44, doi:10.1016/j.jallcom.2012.03.023

[27] C. Xu, T. Nakata, X. G. Qiao, M. Y. Zheng, K. Wu, S. Kamado, Effect of LPSO and SFs on microstructure evolution and mechanical properties of Mg-Gd-Y-Zn-Zr alloy, J. Sci. Rep., 7 (**2017**), 40846, doi:10.1038/srep40846

[28] W. T. Sun, X. G. Qiao, M. Y. Zheng, N. Hu, N. Gao, M. J. Starink, Evolution of long-period stacking ordered structure and hardness of Mg-8.2Gd-3.8Y-1.0Zn-0.4Zr alloy during processing by high pressure torsion, Mater. Sci. Eng., A, 738 (**2018**), 238–252, doi:10.1016/j.msea.2018.09.063

[29] X. J. Zhou, C. M. Liu, Y. H. Gao, S. N. Jiang, Z. Y. Chen, Mechanical Properties of the Mg-Gd-Y-Zn-Zr Alloys with Different Morphologies of Long-Period Stacking Ordered Phases, J. Master. Eng. Perform., 27 (**2018**), 6237–6245, doi:10.1007/s11665-018-3713-z

[30] J. X. Zheng, B. Chen, Interactions between long-period stacking ordered phase and β' precipitate in Mg-Gd-Y-Zn-Zr alloy: Atomic-scale insights from HAADF-STEM, Mater. Lett., 176 (**2016**), 223–227, doi:10.1007/s11665-018-3713-z

[31] Y. Z. Meng, J. M. Yu, K. Liu, H. S. Yu, F. Zhang, Y. J. Wu, Z. M. Zhang, N. N. Luo, H. H. Wan, The evolution of long-period stacking ordered phase and its effect on dynamic recrystallization in Mg-Gd-Y-Zn-Zr alloy processed by repetitive upsetting-extrusion, J. Alloys Compd., 828 (**2020**), 154454, doi:10.1016/j.jallcom.2020.154454

[32] Y. F. Wang, F. Zhan, Y. T. Wang, Y. B. Duan, K. J. Wang, W. J. Zhang, J. Hu, Effect of Zn content on the microstructure and mechanical properties of Mg-Gd-Y-Zr alloys, Mater. Sci. Eng., A, 745 (**2019**), 149–158, doi:10.1016/j.msea.2018.12.088

[33] W. J. Shi, Z. M. Zhang, M. Meng, Y. B. Yang, Effects of homogenization treatment on microstructure and elongation of the Mg-13Gd-4Y-2Zn-0.6Zr alloy, Mater. Res. Express, 5 (**2018**), 016514, doi:10.1088/2053-1591/aaa309